50 years of Strain Analysis JSA

Original Article

J Strain Analysis
2015, Vol. 50(3) 190–198

DOI: 10.1177/0309324714560040
sdj.sagepub.com
SAGE

Experimental characterization and modelling of triaxial residual stresses in straightened railway rails

Robert Kaiser[1], Mario Stefenelli[2], Thomas Hatzenbichler[1], Thomas Antretter[3], Michael Hofmann[4], Jozef Keckes[5] and Bruno Buchmayr[1]

Abstract

Residual stresses in railway rails have a significant influence on the rail functional properties and reliability in service life. Already during the production, the roller straightening as the final production step removing the rail curvature causes the formation of complex stress fields. In this work, a complementary experimental characterization of longitudinal, transversal and normal residual stresses in an uncut straightened rail with a length of 0.5 m is performed using neutron diffraction and contour method. Additionally, the residual stresses are predicted numerically by means of an extensive three-dimensional finite element simulation taking into account the cyclic elastic–plastic material behaviour of the rail including combined kinematic–isotropic hardening. The very good agreement between the experimental and numerical data provides a basis for the understanding and predicting how the straightening procedure, that is, the positioning of the individual rollers and forces applied by the rollers, influences the triaxial stress fields at the rail cross-section.

Keywords

Residual stresses, straightening, simulation, finite element method (FEM), neutron diffraction, contour method

Date received: 16 September 2014; accepted: 14 October 2014

Introduction

Roller straightening is the final step in the production of a railway rail. It follows the cooling to room temperature after the hot rolling performed at about 1000 °C and results in the formation of a rail curvature and relatively small residual stresses[1–3] caused by the specific rail profile geometry and negligible mechanical constrains on the cooling bed. Since most of the rail mass is concentrated in the rails head, the cooling is slower in the head than in the foot. The colder foot and the web exert a longitudinal force on the hot head which leads to a plastic deformation and consequently to a reduction of the rail's length in the head zone. During further cooling, the head cools down and the dimensional mismatch between the foot and the web results in a curvature of the rail whose neutral axis lies near the rail head.

In order to obtain a straight rail, the cooling must be followed by a complex roller straightening process which is performed by alternating bending about the cold rails axes of inertia using a set of rollers (Figure 1). The roller pitch can be regular, like at the horizontal bending machine (HM), or irregular, at the vertical bending machine (VM). Since the straightening step is the final step in the production route, it has a significant influence on the final properties of the rail. As a consequence, the rail should not only be straight, but residual stresses should be minimal after this process.[4] According to a draft standard elaborated by European Committee for Standardization (CEN), the longitudinal residual stresses in the middle of the rail foot must not exceed 250 MPa.[5]

In order to quantify residual stresses in rails, numerous experimental and computational works have been performed in the past.[3,4,6–21] Pioneering studies

[1]Chair of Metal Forming, Montanuniversitaet Leoben, Leoben, Austria
[2]Materials Center Leoben Forschung GmbH, Leoben, Austria
[3]Institute of Mechanics, Montanuniversitaet Leoben, Leoben, Austria
[4]FRM II, TU München, Munich, Germany
[5]Chair of Materials Physics, Montanuniversitaet Leoben, Leoben, Austria

Corresponding author:
Jozef Keckes, Chair of Materials Physics, Montanuniversitaet Leoben, Franz-Josef-Strasse 18, Leoben, Austria.
Email: jozef.keckes@gmail.com

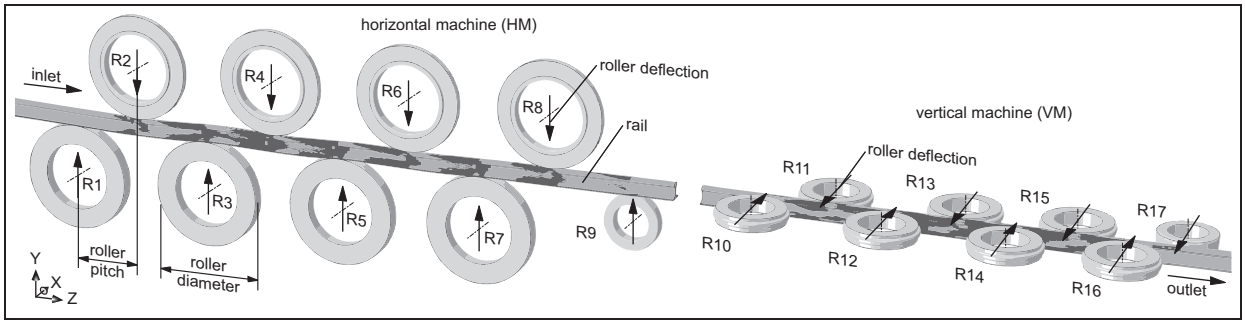

Figure 1. A schematic sketch of the straightening process performed by the horizontal (HM) and vertical (VM) machines. The arrows indicate deflection of selected rollers. The dark grey regions on the rail indicate the plastic deformation zone.

appeared already in 1937 by Meier[3] where the typical C-shaped residual stress distribution for straightened rails characterized by sectioning methods was recognized. More recent publications[6–12,14–16,22,23] were devoted to non-destructive volume-sensitive stress characterization using neutrons and synchrotron radiation. Sasaki et al.[10] used neutron diffraction to evaluate residual stresses in small sections of 10 mm of a rail head. Similarly, Jun et al.[11] performed neutron diffraction measurements on a 16-mm-thick transverse slice through the entire profile of a rail which has been in service. In order to eliminate the effect of the sectioning, Luzin et al.[12,22] characterized residual stresses in a 10-mm-thick rail section and in a 0.5-m-long rail. The results documented that the sectioning results in the significant modification of the original residual stresses in the rail where especially longitudinal stress components were affected.

Another approach to evaluate longitudinal residual stresses in rail long sections is the contour method proposed by Prime and colleagues.[24–26] The specimen is cut in two pieces normal to the profile axis, which leads to an elastic recovery of the longitudinal stresses. The stresses can be calculated from the relaxation strains by a variation of Bueckner's superposition principle[27] or by finite element modelling.[25] Prime[24,25] shows, based on the example of a bent beam specimen, that this method can measure a full two-dimensional (2D) map of the residual stress component normal to the cross-section. Knowing that the longitudinal residual stress is the most critical component for railway rails makes this method an interesting alternative, even though only one stress component can be evaluated.

Residual stresses in railway rails have been characterized primarily in used rail sections in order to evaluate the influence of the service on the stress development.[7,8,11,12,15,16] The experimental stress characterization in 'as-produced' rails with preserved longitudinal components, that is, in an unsectioned rail, has not been performed yet. There have been however a few approaches to determine the stress state in straightened rails using FEM. One approach is based on the classical Euler–Bernoulli assumptions for bending in combination of the theory of Hertz to model the stress evolution in the rails cross-sections during straightening influenced by the roller contact.[17,18] In other models, 2D or three-dimensional (3D) modelled sections of the rail are driven by boundary conditions calculated from the bending line analytically or by a beam model. In that case, the influence of the contact situation was also modelled supposing elastic or rigid rollers.[4,19,20,28,29]

The objectives of this work are (1) to perform an experimental characterization of residual stresses in an uncut straightened rail of steel grade R260 and rail profile 60E1[5] (with unrelaxed longitudinal residual stresses) using neutron diffraction and the contour method and (2) to correlate the results with a finite element simulation of the straightening process. Finally, the combination of experimental and numerical approaches allows (1) a validation of the model and (2) also the understanding and the optimization of the straightening procedure. Methodologically, the approach should also evaluate the advantages and disadvantages of stress characterization using neutrons and the contour method in large engineering components.

Experimental

Neutron diffraction characterization

Residual stress characterization was performed in a straightened 0.5-m-long rail with the preserved original stress state at the Stress-Spec neutron diffractometer[30] of the FRMII facility in Garching, Germany. The details of the experimental setup and the technique can be found in Jun et al.,[11] Hofmann et al.[30] and Hutchings et al.[31] For the measurements, a neutron wavelength of 1.664 Å and a gauge volume of $5\times5\times5$ mm^3 were used. The gauge volume was defined by a slit in the incoming beam and a radial collimator before the detector to leave enough space for the large sample. The reason for the relatively large gauge volume was the low neutron transmission of about 1%–2% forints in the head, that resulted in low diffraction statistics and long coating times of up to 2 h per acquisition.[22] The diffraction signal was recorded using a 2D detector with an active area of 300×300 mm^2 and a pixel size of about 1.4 mm.

For the position-resolved characterization of diffraction elastic strains $\varepsilon_i^{hkl}(x,y,z)$ in the rail at the positions (x,y,z), α-Fe hkl reflections 211 or 110 were scanned with diffraction vectors oriented parallel to the transverse, normal and longitudinal rail axes. The main reasons to select Fe 211 and 110 reflections for the strain analysis were that (1) the diffraction angles were easily accessible by the 2D neutron detector, (2) the reflections exhibit a low sensitivity to intergranular strains of second and third order and (3) the diffraction elastic constants do not differ significantly. The 110 reflections were used to measure the points in the head, as the lower Bragg angle of 48° and additional tilting of the sample would allow shorter pathways. Most of the measurement points were located along the rail vertical symmetry axis. The measured diffraction angles were used to calculate the lattice spacing $d_i^{hkl}(x,y,z)$ using Bragg's law. The unstressed lattice parameters d_0^{hkl} were determined experimentally by measuring $4\times4\times4\,\mathrm{mm}^3$ steel cubes extracted from the rail. The diffraction elastic strain in three directions was determined according to

$$\varepsilon_i^{hkl}(x,y,z) = \frac{d_i^{hkl}(x,y,z) - d_0^{hkl}(x,y,z)}{d_0^{hkl}(x,y,z)} \quad (1)$$

where i represents the transverse (x), normal (y) and longitudinal (z) orientations of the diffraction vector. The triaxial residual stresses at the positions (x,y,z) were determined using

$$\sigma_i(x,y,z) = \frac{E^{hkl}}{(1+\nu^{hkl})} \left(\varepsilon_i^{hkl}(x,y,z) + \frac{\nu^{hkl}}{(1-2\nu^{hkl})} \left(\varepsilon_x^{hkl}(x,y,z) + \varepsilon_y^{hkl}(x,y,z) + \varepsilon_z^{hkl}(x,y,z) \right) \right) \quad (2)$$

where a Young's modulus of $E^{hkl} = 216\,\mathrm{GPa}$ and a Poisson's ratio of $\nu^{hkl} = 0.286$ were used for both reflections.[32]

Contour method

The contour method[24,25,33] was applied to characterize residual stresses in an as-produced roller-straightened rail, having a length of 0.5 m. The cut was carried out by a conventional industrial wire electric discharge machining (WEDM) machine approximately in the rail centre and perpendicular to the rail longitudinal axis. After the cutting, both cutting surfaces were scanned using a coordinate measuring machine (CMM), applying a grid of $1\times1\,\mathrm{mm}^2$. In order to obtain accurate results, the measured contour was corrected to compensate errors from the cutting process. According to Prime and Kastengren,[33] there are anti-symmetric and symmetric errors. The first group derives from the effects such as shifting of the parts due to bad clamping or a crooked cut, and can be corrected by averaging the contours of both cutting surfaces. The latter group comprises local variations in the cutting surfaces due to the cutting itself, such as changes in the cut width.[34–36] These errors can be corrected by subtracting the contour obtained from a stress-free reference.[33,37]

To determine the *unknown* 2D residual stress distribution across the as-produced rail from the *known* measured and corrected 2D contour data, an elastic finite element model was used applying Young's modulus $E = 205\,\mathrm{GPa}$ and the Poisson's ratio $\nu = 0.3$. In the model, numerical contour data equivalent to those from the experiment were generated on a 0.25-m-long rail segment and then the curved rail cross-section was displaced to the plane state. The 2D stress generated in the rail using the later step was considered as the searched residual stress in the uncut as-produced rail.

FEM analysis of the straightening process

The roller straightening process of the rail was modelled with FEM using Abaqus/Standard.[38] For the cyclic elastic–plastic material behaviour of the rail steel, the already implemented Chaboche model was used.[38–40] The parameters for the model were extracted from experimental cyclic mechanical tests performed on the rail material using strains in the range of 0.5%–1.0%. Additionally, unsymmetrical stress-controlled cyclic tests were used to adjust the ratcheting behaviour.

To reduce the numbers of elements in the 3D model of the straightening process, a sub-modelling technique was used. This entails performing the numerical analysis in two steps: (1) a global analysis, where a simple beam element model of the rail is generated and pulled through the roller straightener, and where the history of the displacements and rotations of each node is monitored, (2) the subsequent submodel analysis, where a designated section of interest is finely meshed using 3D solid elements whose bounding plane positions are subjected to the nodal displacement and rotation history calculated in the global analysis. The model provides the possibility to define an initial stress state and consequently also an initial rail curvature. The results obtained from the model (and also experimental measurements performed on an unstraightened rail) revealed that the rail curvature and also the residual stress state after the cooling down before the straightening have negligible influence on the final residual stress state in the straightened rail.[37]

To prevent shear locking of the elements during bending, the 3D solid eight-node linear brick element with reduced integration (C3D8R) was used. The rollers were modelled as rigid. For the contact model, Coulomb friction ($\mu = 0.15$)[41] was assumed. The compliance of the roller surface was accounted for by a so-called softened contact relationship. For this purpose, the pressure–overclosure relationship was defined by the contact stiffness derived from the Hertz theory.[42,43]

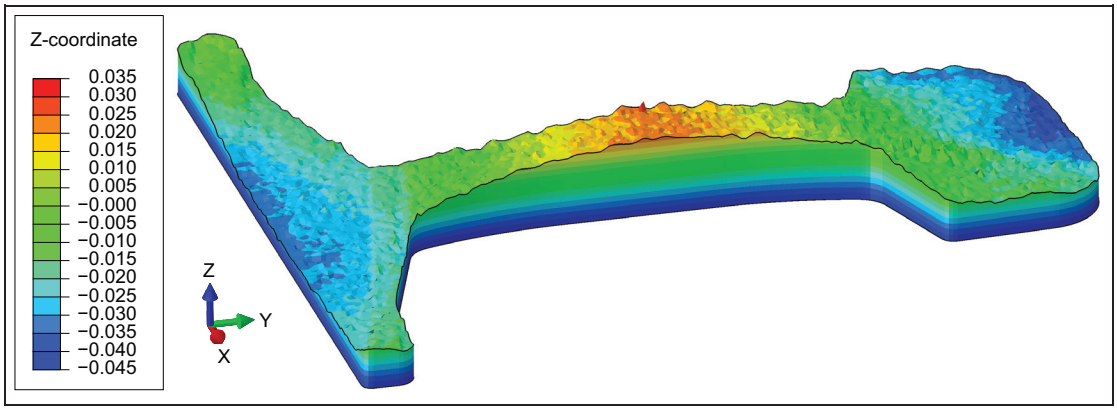

Figure 2. Displacement data in millimetre obtained using the contour method indicate the local material relaxation across the rail cross-section after the cutting. Positive and negative values correspond to compressive and tensile longitudinal stresses.

The calculation time for the 170,000 elements containing submodel was about 240 h on 12 processors.

Results and discussion

Contour data

The characterization of the 2D distribution of the longitudinal stresses across the annealed rail with a grid of 1×1 mm^2 was performed using the contour method. In Figure 2, the experimental data obtained from a CMM after error elimination are presented. The displacement values in the range from -0.045 to 0.035 mm indicate the presence of compressive and tensile stresses at the rail cross-section.

The contour data from Figure 2 were used to evaluate longitudinal stresses using the FEM model (cf. section 'Contour method'). The results in Figure 3 indicate the presence of a C-like longitudinal stress profile across the rail cross-section with about 160 and 130 MPa at the foot and head, respectively, and -125 MPa in the web. The tensile stresses obtained from the contour approach are significantly smaller than the strength of the material and lie obviously also within the limit defined by the CEN draft standard of 250 MPa. The error of the contour method in the residual stress determination is very difficult to quantify. After considering the uncertainties during the sample preparation and the characterization as well as the evaluation procedure, it is believed that the experimental error is smaller than $\pm15\%$.

Neutron residual stress characterization

Neutron diffraction allows characterizing all three stress components in the rail. Due to the long pathways in the material and the resulting long measurement times, the triaxial stresses were determined only in selected volume elements with the size of $5\times5\times5$ mm^3. Longitudinal residual stresses for selected probe positions are presented in Figure 4. Additionally, triaxial residual stresses along the rail symmetry axis are shown in Figure 5.

Also in the case of neutron characterization, longitudinal tensile stresses of 160 and 130 MPa were observed in the foot and head, respectively, whereas a stress of -125 MPa was determined in the web centre. The magnitudes of the stresses determined in the head are comparable with the results of Jun et al.[11] where actually stress reconstruction from measurements on thin rail slices was used. The relatively large measurement errors from about 20 MPa in the web centre to about 80 MPa in the rail head were caused especially by the long pathways of the neutrons which resulted in relatively weak diffraction statistics. The last measurement points in the foot (at 3 mm) and head (at 170 mm) show an abrupt change in stress, which also violates the boundary condition of σ_y being zero at the surface. These stresses can be considered artefacts due to surface effects, as at these points, the gauge volume was not fully immersed into the material.[44]

FEM modelling

The FEM model was used to determine the distribution of triaxial stresses at the rail cross-section after the straightening (Figure 6). The results indicate again a C-like shape of the longitudinal stresses (Figure 6(c) and (d)) with the stress profile varying in the range of about -75 to 100 MPa. The medium transversal and normal compressive stresses of about -60 MPa in the rail head near the surface were formed during an unloading of the rollers after the roller contact was removed. The region of transversal tensile stresses in the head is caused by the higher compressive deformation by the rollers of the VM in contrast to the lateral region (Figure 6(a)). The same effect, however in normal direction, is caused by the upper role of the HM (Figure 6(b)).

The C-profile can easily be interpreted by analysing the individual modelling steps of the straightening process. During the first rail bending under the roll number R2 (cf. Figure 1), longitudinal compressive stresses form in the head and tensile stresses in the foot, large enough that plastification occurs leaving residual

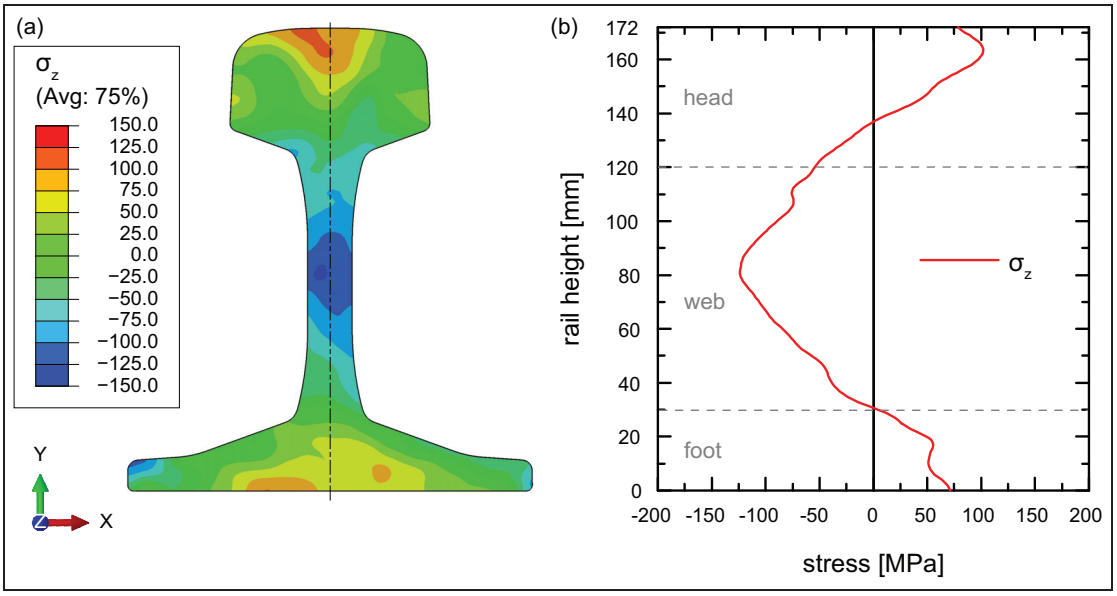

Figure 3. Two-dimensional distribution of longitudinal residual stresses σ_z across the straightened rail (a) determined by means of the contour method and the stress profile across the rail vertical axis (b).

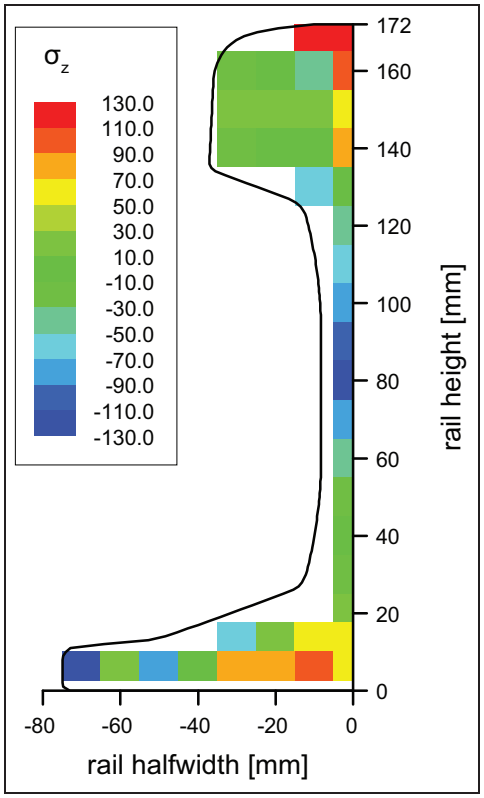

Figure 4. Longitudinal residual stresses in MPa across the straightened rail determined using neutron diffraction.

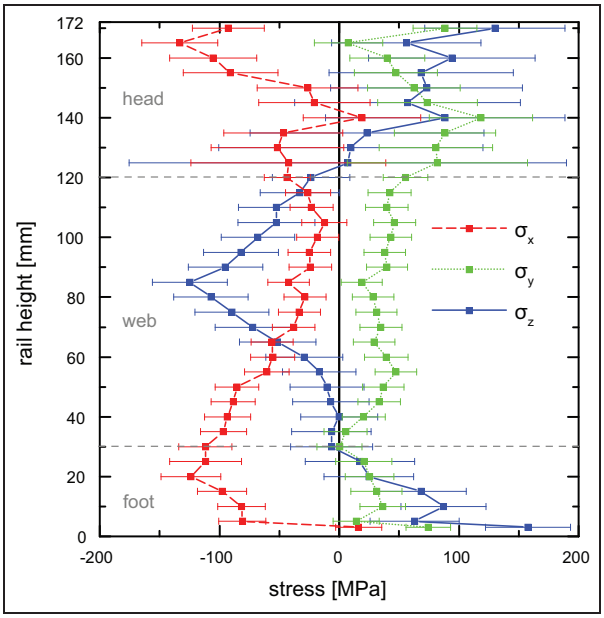

Figure 5. Distribution of triaxial stresses in the straightened rail across the rail symmetry vertical axis determined by neutron diffraction.

stresses with an opposite sign after unloading between R2 and R3. This means that before entering R3, the head is exposed to tensile and the foot to compressive residual stresses. Bending about R3 basically reverses the situation, however to a lesser extent as the positioning of the rolls is chosen in such a way that the rail's curvature radii decay as the rail progresses towards the end of the roller straightener. At this point, it is important to note that the intricate contact situation between the roll and the rail introduces a significant amount of plasticity in the outer fibre of the rail that can only be accommodated by a widening of the rail (i.e. a material flow in the x-direction, cf. Figure 1) due to the kinematic constraints in the other directions. The Poisson effect then generates tensile stresses in the z-direction that add to the stresses due to bending. This is repeated every time the rail is bent upwards or downwards.

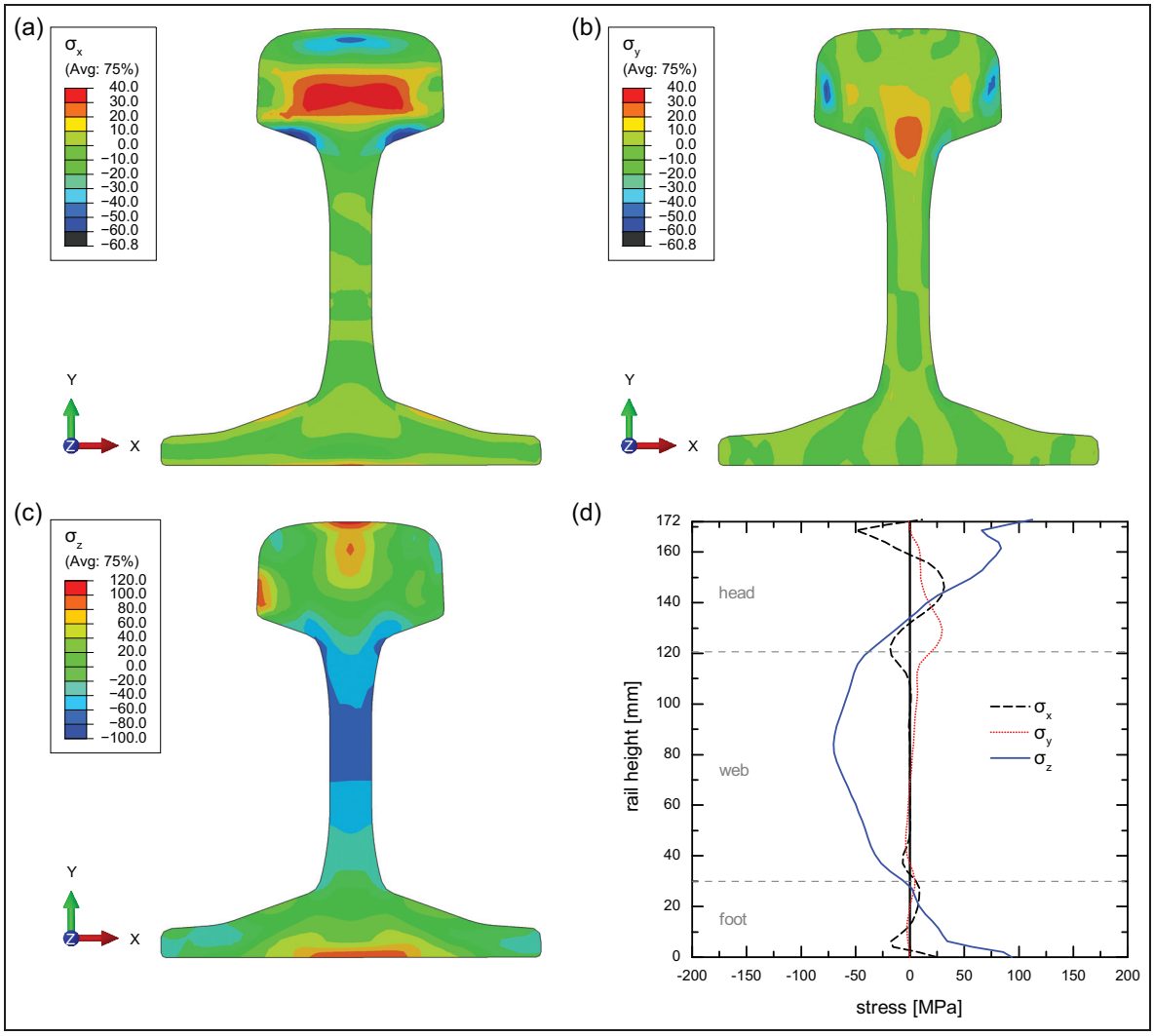

Figure 6. Spatial distribution of (a) transversal σ_x, (b) normal σ_y and (c) longitudinal σ_z stresses across the rail cross-section, as obtained from the FEM model. (d) Distribution of triaxial stresses along the rail symmetry axis.

These additional tensile stresses are equilibrated by compressive stresses in the web of the rail giving rise to the characteristic C-shaped longitudinal stress distribution that is commonly observed in roller-straightened beams. Speaking in terms of strains, this phenomenon can also be explained by a steady reduction of the beam length with every bending. This reduction can actually be measured amounting to about 100 mm for a 60-m rail after leaving the roller straightener. The formation of the C-profile is an inevitable consequence of the additional plasticity underneath the rolls and hence the entire straightening process. Changing process parameters will only shift or flatten this C-shaped stress distribution. The finite element model offers a cost-effective method to adjust the process parameters such as to minimize the magnitudes of the tensile stresses at the head and at the foot.

Results comparison

One of the main objectives of this work was to analyse longitudinal residual stresses in the as-produced straightened rail. The longitudinal residual stress from the contour method, neutron diffraction and FEM approach are presented in Figure 7. As already documented in sections 'Contour data', 'Neutron residual stress characterization', 'FEM modelling' and 'Results comparison', the longitudinal stress distributions exhibit always a C-like profile which was confirmed by all three methods. Although the magnitudes of the stress dependencies differ by about 50 MPa, the common trend of compressive stresses in the web and tensile stresses in the head and foot is obvious.

Discussion

The combination of two experimental techniques and the FEM modelling procedure demonstrated that all three approaches provide qualitatively the same profile of the longitudinal stresses across the rail vertical axis with a typical 'C' shape. The tensile longitudinal residual stresses in Figure 7 are significantly smaller than the strength of the material and lie obviously also within the limit defined by the CEN draft standard of

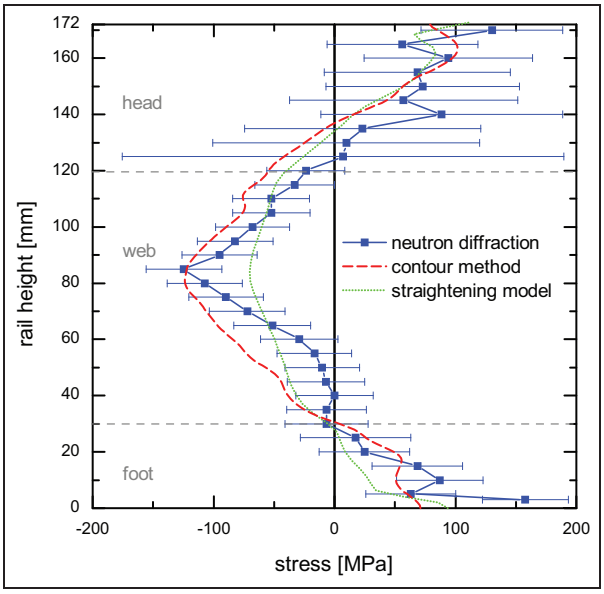

Figure 7. Comparison of the longitudinal residual stress σ_z distribution along the vertical symmetry axis evaluated by the contour method, neutron diffraction and FEM approach.

250 MPa. The aim of this paragraph is to discuss the individual approaches.

The contour method provided representative data on the longitudinal stresses which agree very well with the values obtained from other techniques (Figure 7). The whole procedure including sample preparation, surface mapping and data processing takes about 20 h. The main advantages of the technique are the relative cost-effectiveness and the fact that the method provides 2D distribution of the stresses across the rail cross-section with a mesh of 1×1mm (Figure 2). As drawbacks, one should mention that a contour of a stress-free reference must be measured additionally in order to correct for measurement errors, and a linear elastic 3D finite element model must be built in order to reconstruct the residual stress fields from the measurement displacement fields.

In the case of neutron characterization, the measurements can be performed on an as-delivered rail of 0.5 m in length without the need of cutting. Due to the long pathways resulting in a bad diffraction statistics and acquisition times up to 2 h, a relatively large probing volume of $5\times5\times5$ mm^3 was used. This allowed to reduce the measurement time to as low as 4 days. This demonstrates that this type of analysis is restricted to dedicated samples only, because it is expensive and must be planned in advance. Similar as in the case of contour method, also for the neutron characterization, stress-free samples must be provided in order to determine unstressed lattice parameters of the crystal. The rail length of 0.5 m proved to be long enough in order to preserve the longitudinal stress components.

The FEM analysis provided very detailed data on the stress distribution across the rail. The predictive quality of such an approach relies however on the accuracy of the material model which has to be able to account for cyclic plasticity including the hardening mechanisms that are relevant within the first loading cycles. Determining the pertaining material parameters requires cyclic tension-compression tests at strain amplitudes similar to the actual straightening process. Particular attention has also to be paid to the details of the contact between the rail and the roll as this has a significant influence on the stress situation especially in the outer fibres. Once a reliable model is set up, sufficiently large computational resources must be provided. In the present case, the two-step simulation (global model and submodel) of the process took 2 weeks on 12 standard x86 3-GHz cores. The main advantage of the FEM approach is naturally the fact that once the numerical method has been validated against the experimental evidence, it may unfold its strength by providing full versatility with respect to parameter variations, such as different roller positions or forces applied by the individual rollers. The comparison of the results obtained from the straightened and unstraightened rails has revealed that the curvature and also residual stress state after the cooling down have negligible influence on the final residual stress state in the straightened rail.

Conclusion

The longitudinal residual stress distribution across the vertical axis of the straightened rail was characterized using neutron diffraction, the contour method and a FEM model. All three approaches delivered the same stress profile with a typical ‘C’ shape and the maximal tensile stresses below the limit of 250 MPa defined by the CEN draft standard. Methodologically, the work demonstrates that all three approaches provide actually equivalent results which were however achieved using absolutely different procedures and also under very different costs.

The validation and adjustment of the FEM approach with the experimental data represents an important step in understanding and control of the straightening process. The development of the FEM approach opens the way to produce rails with well-adjusted residual stress fields by varying roller positions or forces applied by the individual rollers.

Declaration of conflicting interests

The authors declare that there is no conflict of interest.

Funding

This study was financially supported by the Austrian Federal Government (in particular from Bundesministerium für Verkehr, Innovation und Technologie and Bundesministerium für Wissenschaft, Forschung und Wirtschaft) represented by Österreichische Forschungsförderungsgesellschaft mbH

and the Styrian and the Tyrolean Provincial Government, represented by Steirische Wirtschaftsförderungsgesellschaft mbH and Standortagentur Tirol, within the framework of the COMET Funding Programme.

This research project has been supported by the European Commission under the 7th Framework Programme through the 'Research Infrastructures' action of the 'Capacities' Programme, Contract No.: CP-CSA_INFRA-2008-1.1.1 Number 226507-NMI3.

References

1. Hinteregger E. *Eigenspannungen und Verformungen in Schienen nach dem Walzen vor dem Richten*. Leoben: Montanuniversität Leoben, 1990.
2. Hinteregger E, Fischer FD, Rammerstorfer FG, et al. Berechnung der Längseigenspannungen langer Schienen während des Abkühlens. *BHM* 1990; 135(11): 437–442.
3. Meier H. Eigenspannungen in Eisenbahnschienen. *Z Ver Dtsch Ing* 1937; 81(12): 362–363.
4. Schleinzer G and Fischer FD. Residual stresses in new rails. *Mater Sci Eng A* 2000; 288(2): 280–283.
5. Bahnanwendungen – Oberbau - Schienen – Teil 1: Vignolschienen ab 46 kg/m. Deutsche Fassung EN 13674-1:2003 + A1:2007, 2008.
6. Hirao M, Ogi H and Fukuoka H. Advanced ultrasonic method for measuring rail axial stresses with electromagnetic acoustic transducer. *Res Nondestruct Eval* 1994; 5(3): 211–223.
7. Webster PJ, Hughes DJ, Mills G, et al. Synchrotron X-ray measurements of residual stress in a worn railway rail. *Mater Sci Forum* 2002; 404–407: 767–772.
8. Buttle DJ, Dalzell W and Thayer PJ. Nondestructive residual stress measurement in rail heads and rolling contact fatigue. *Insight* 2002; 44(6): 364–368.
9. Magiera J. Enhanced 3D analysis of residual stress in rails by physically based fit to neutron diffraction data. *Wear* 2002; 253(1–2): 228–240.
10. Sasaki T, Takahashi S, Kanematsu Y, et al. Measurement of residual stresses in rails by neutron diffraction. *Wear* 2008; 265(9–10): 1402–1407.
11. Jun TS, Hofmann F, Belnoue J, et al. Triaxial residual strains in a railway rail measured by neutron diffraction. *J Strain Anal Eng* 2009; 44(7): 563–568.
12. Luzin V, Gnaupel-Herold T, Gordon JE, et al. Neutron residual stress measurements on rail sections for different production conditions. In: *Proceedings of IMECE*, Anaheim, CA, 2004, pp.117–122. ASME.
13. Withers PJ, Turski M, Edwards L, et al. Recent advances in residual stress measurement. *Int J Pres Ves Pip* 2008; 85(3): 118–127.
14. Webster GA and Ezeilo AN. Residual stress distributions and their influence on fatigue lifetimes. *Int J Fatigue* 2001; 23(Suppl. 1): 375–383.
15. Kelleher J, Prime MB, Mummery PM, et al. The measurement of residual stress in railway rails by diffraction and other methods. *J Neutron Res* 2003; 11(4): 187–193.
16. Kelleher JF, Buttle DJ, Mummery PM, et al. Residual stress mapping in railway rails. *Mater Sci Forum* 2005; 490–491: 165–170 (7th international conference on residual stresses (ICRS-7); Conference code: 70365).
17. Guericke W. Modell zur Simulation elastisch-plastischer Biegeverformungen für technologische Bearbeitungsprozesse. *Technische Mechanik* 1994; 14(2): 155–176.
18. Weiser J. *Analyse der Eigenspannungsentstehung beim Rollenrichten von Schienen*. Magdeburg: Otto-von-Guericke-Universität Magdeburg, 1997.
19. Finstermann G, Fischer FD, Shan G, et al. Residual stresses in rails due to roll straightening. *Steel Res* 1998; 69(7): 272–278.
20. Schleinzer G. *Residual stress formation during the roller straightening of rails*. Leoben: Montanuniversität Leoben, 2000.
21. Schleinzer G and Fischer FD. Residual stress formation during the roller straightening of railway rails. *Int J Mech Sci* 2001; 43(10): 2281–2295.
22. Luzin V, Prask HJ, Gnaupel-Herold T, et al. Neutron residual stress measurements in rails. *Neutron News* 2013; 24(3): 9–13.
23. Song X and Korsunsky AM. Fully two-dimensional discrete inverse eigenstrain analysis of residual stresses in a railway rail head. *J Appl Mech* 2011; 78(3): 031019 (6 pp.).
24. Prime MB. The contour method: simple 2-D mapping of residual stresses. *Am Soc Mech Eng Pres Ves P* 2000; 415: 121–127.
25. Prime MB. Cross-sectional mapping of residual stresses by measuring the surface contour after a cut. *J Eng Mater: T ASME* 2001; 123(2): 162–168.
26. Pagliaro P, Prime MB, Swenson H, et al. Measuring multiple residual-stress components using the contour method and multiple cuts. *Exp Mech* 2010; 50: 187–194.
27. Buenckner HF. The propagation of cracks and the energy of elastic deformation. *J Appl Mech: T ASME* 1958; 80: 1225–1230.
28. Varney BE and Farris TN. Mechanics of roller straightening. In: *39th mechanical working and steel processing conference*, Indianapolis, IN, USA, 19–22 October 1997, vol. 35, pp. 1111–1121, Warrendale, PA: Iron & Steel Soc of AIME.
29. Betegón Biempica C, del Coz Díaz JJ, García Nieto PJ, et al. Nonlinear analysis of residual stresses in a rail manufacturing process by FEM. *Appl Math Model* 2009; 33(1): 34–53.
30. Hofmann M, Schneider R, Seidl GA, et al. The new materials science diffractometer STRESS-SPEC at FRM-II. *Physica B* 2006; 385–386: 1035–1037 (Proceedings of the eighth international conference on neutron scattering).
31. Hutchings MT, Withers PJ, Holden TM, et al. *Introduction to the characterization of residual by neutron diffraction*. Boca Raton, FL: CRC Press/Taylor & Francis, 2005.
32. Kim SA and Johnson WL. Elastic constants and internal friction of martensitic steel, ferritic-pearlitic steel, and α-iron. *Mater Sci Eng A* 2007; 452–453: 633–639.
33. Prime MB and Kastengren AL. The contour method cutting assumption: error minimization and correction. In: T Proulx (ed.) *Experimental and applied mechanics*, vol. 6 (Conference proceedings of the society for experimental mechanics series). New York: Springer, 2011, pp.233–250.
34. Tosun N, Cogun C and Tosun G. A study on kerf and material removal rate in wire electrical discharge machining based on Taguchi method. *J Mater Process Tech* 2004; 152(3): 316–322.

35. Di S, Chu X, Wei D, et al. Analysis of kerf width in micro-WEDM. *Int J Mach Tool Manu* 2009; 49(10): 788–792.
36. Alias A, Abdullah B and Abbas NM. Influence of machine feed rate in WEDM of titanium Ti-6Al-4V with constant current (6A) using brass wire. *Procedia Eng* 2012; 41: 1806–1811 (International Symposium on Robotics and Intelligent Sensors 2012, IRIS 2012).
37. Kaiser R. *Eigenspannungsoptimiertes Richten von Eisenbahnschienen*. Leoben: Montanuniversitaet Leoben, 2014.
38. *Abaqus 6.12 documentation*. Providence, RI: Dassault Systèmes SIMULIA Corporation, 2012.
39. Chaboche JL. Constitutive equations for cyclic plasticity and cyclic viscoplasticity. *Int J Plasticity* 1989; 5(3): 247–302.
40. Lemaitre J and Chaboche JL. *Mechanics of solid materials*. Cambridge University Press, 2000.
41. Hensel A, Poluchin PI and Poluchin WP (eds). *Technologie der Metallformung Eisen- und Nichteisenwerkstoffe*. 1st ed.Leipzig: Deutscher Verlag für Grundstoffindustrie, 1990.
42. Kaiser R, Hatzenbichler T, Buchmayr B, et al. Simulation of the roller straightening process with respect to residual stresses and the curvature trend. *Mater Sci Forum* 2014; 768–769: 456–463.
43. Hertz H. Über die Berührung fester elastischer Körper. *Journal für die reine und angew Math* 1881; 92: 156–171.
44. Webster PJ, Mills G, Wang XD, et al. Impediments to efficient through-surface strain scanning. *J Neutron Res* 1996; 3(4): 223–240.